Available online at www.sciencedirect.com
ScienceDirect
Trans. Nonferrous Met. Soc. China 32(2022) 3362−3373
Transactions of Nonferrous Metals Society of China
www.tnmsc.cn

Empirical decay relationship between ionic conductivity and porosity of garnet type inorganic solid-state electrolytes

Zhi-hao GUO[1,2,3], Xin-hai LI[1,2,3], Zhi-xing WANG[1,2,3], Hua-jun GUO[1,2,3], Wen-jie PENG[1,2,3], Qi-yang HU[1,2,3], Guo-chun YAN[1,2,3], Jie-xi WANG[1,2,3]

1. School of Metallurgy and Environment, Central South University, Changsha 410083, China;
2. Engineering Research Center of the Ministry of Education for Advanced Battery Materials, Central South University, Changsha 410083, China;
3. Hunan Provincial Key Laboratory of Nonferrous Value-added Metallurgy, Central South University, Changsha 410083, China

Received 6 September 2021; accepted 19 December 2021

Abstract: Ionic conductivity is one of the crucial parameters for inorganic solid-state electrolytes. To explore the relationship between porosity and ionic conductivity, a series of $Li_{6.4}Ga_{0.2}La_3Zr_2O_{12}$ garnet type solid-state electrolytes with different porosities were prepared via solid-state reaction. Based on the quantified data, an empirical decay relationship was summarized and discussed by means of mathematical model and dimensional analysis method. It suggests that open porosity causes ionic conductivity to decrease exponentially. The pre-exponential factor obeys the Arrhenius Law quite well with the activation energy of 0.23 eV, and the decay constant is averaged to be 2.62%. While the closed porosity causes ionic conductivity to decrease linearly. The slope and intercept of this linear pattern also obey the Arrhenius Law and the activation energies are 0.24 and 0.27 eV, respectively. Moreover, the total porosity is linearly dependent on the open porosity, and different sintering conditions will lead to different linear patterns with different slopes and intercepts.

Key words: garnet type solid-state electrolyte; ionic conductivity; porosity; empirical decay relationship

1 Introduction

Lithium-ion batteries are marvelous electrochemical energy-storage devices which have been widely applied in portable electronic devices and possess great potential for the large-scale application in electric transportation and smart grid areas [1−3]. However, the current energy density of lithium-ion batteries cannot satisfy the increasing demand [4−6]. One of the promising methods to further safely improve its energy density is to develop solid-state lithium-ion batteries [7,8]. Solid-state electrolytes lie at the heart of the solid-state battery concept [9,10]. Compared with organic solid-state electrolytes, inorganic solid-state electrolytes are superior in terms of ionic conductivity and electrochemical window and have great potential to be utilized in solid-state lithium-ion batteries [11,12].

Ionic conductivity is one of the crucial parameters for inorganic solid-state electrolytes [13]. Generally speaking, denser electrolytes exhibit higher ionic conductivity. For argyrodite type $Li_{6.6}P_{0.4}Ge_{0.6}S_5I$, KRAFT et al [14] reported that the ionic conductivity could rise from 5.4 mS/cm in a cold-pressed state to 18.4 mS/cm upon sintering, which could be attributed to better grain contact of the densification process. This work reveals the importance of densifying solid-state electrolytes

Corresponding author: Xin-hai LI, Tel: +86-13973168798, E-mail: xinhaili_csu@126.com
DOI: 10.1016/S1003-6326(22)66025-4

for higher ionic conductivity but the comparison experiment is qualitative. A quantitative comparison example is that the ionic conductivity increases from 14 to 25 mS/cm when the relative density is improved from 75% to 90% for Thio-LISICON type $Li_{9.54}Si_{1.74}P_{1.44}S_{11.7}Cl_{0.3}$ [15]. As for oxide materials, densification of solid-state electrolytes is also vital for higher ionic conductivity. For the well-known NASICON type material, AONO et al [16] suggested that the conductivity enhancement of $LiTi_2(PO_4)_3$ by the substitution or by the binder addition resulted mainly from the densification of the sintered pellets. For garnet type $Li_{6.75}La_3Zr_{1.75}Ta_{0.25}O_{12}$, ZHANG et al [17] reported that the ionic conductivity at room temperature was enhanced to 0.69 mS/cm with the relative density of the pellet as 92%. However, relative density is an overall item to describe the level of densification. In reality, there exist open porosity and closed porosity. Just recently, reduced open porosity has been considered as the reason for higher Li-ion conductivity of the non-sintered garnet type solid electrolyte LLZTO-xLiBH$_4$ ($0 \leq x \ll 4$) [18]. These reports suggest the importance of densifying electrolytes for higher ionic conductivity, but the concrete relationship of open porosity, closed porosity and ionic conductivity is still unclear. Moreover, the method of measuring relative density from these works is not clearly given.

Garnet type inorganic solid-state electrolyte is a well-known material and posseses great potential for the application in solid-state lithium-ion batteries [10]. In this work, with nominal chemical composition $Li_{6.4}Ga_{0.2}La_3Zr_2O_{12}$ as a case study, a series of electrolytes with different porosities were prepared under different sintering conditions to explore the relationship between porosity and ionic conductivity. Based on the quantified data, an empirical decay relationship was summarized and discussed by means of mathematical model and dimensional analysis method. Meanings and limitations of this summarized model were also summarized and discussed.

2 Experimental

2.1 Synthesis of solid-state electrolytes

The nominal chemical composition $Li_{6.4}Ga_{0.2}La_3Zr_2O_{12}$ solid-state electrolytes were prepared by typical powder-covering solid-state sintering [19]. Stoichiometric Li_2CO_3 (99%, Aladin) (10% excess to compensate potential lithium loss during sintering), Ga_2O_3 (99.99%, Aladin), La_2O_3 (99.99%, Sinopharm) and ZrO_2 (99%, Sinopharm) were planetary mill-balled for 8 h at a rotation speed of 250 r/min with isopropanol (AR, Macklin) as liquid medium. The mixture was then dried and calcinated in MgO crucibles at 950 °C for 8 h. The calcinated powder was ball-milled for 10 h at a rotation speed of 250 r/min and dried. The resulting fine powder was pressed under 150 MPa to be green-ware pellets with a diameter of 18 mm and a thickness of around 4 mm. The pellets were then sintered in MgO crucibles and covered with undoped $Li_7La_3Zr_2O_{12}$ as cover powder. Samples prepared under different sintering conditions were named in the form of "sintering temperature-sintering duration-M" or "sintering temperature-sintering duration-T", for instance, "1250°C-32h-M" and "1250°C-32h-T". It should be noted that the samples with suffix "M" were employed to create a model, while the samples with suffix "T" were meant to verify the as-summarized model.

2.2 Structural, morphology and porosity characterization

The crystal structure of the pellets was identified by XRD with Cu K_α with Empyrean 2 (Netherlands PANalytical). The microstructure and cross-section morphology of pellets were observed by SEM with JSM−7900F (Japan JEOL). The chemical composition was determined by inductively coupled plasma optical emission spectroscopy (ICP-OES) with Spectro Blue Sop (Germany Spectro).

Pycnometry was carried out as following procedures. Firstly, the as-prepared pellet was soaked and boiled in isopropanol for 3 h, and then it was taken out from the container and put in a pycnometer. Afterwards, the pycnometer was filled with isopropanol to its full state. m_1 is the total mass of the pellet and pycnometer with full isopropanol. Secondly, the pellet was taken out from the pycnometer. The extra residuary liquid on the surface of pellet was wiped off with delicate tissue paper carefully. The mass of this wet pellet was measured as m_w. Thirdly, wet pellet was then dried until the mass of it did not change. The mass of this dry pellet was measured as m_d. Lastly, m_2 was the total mass of the same pycnometer with full

isopropanol. ρ_{ISO} was the density of isopropanol. Thus, the apparent density (D_a), volume density (D_V) and open porosity (P_O) were identified by pycnometry with isopropanol as medium based on the following equations.

$$D_a=\rho_{Iso}m_d/[(m_d-(m_1-m_2)] \quad (1)$$

$$D_V=\rho_{Iso}m_d/[(m_w-(m_1-m_2)] \quad (2)$$

$$P_O=(m_w-m_d)/[m_w-(m_1-m_2)] \quad (3)$$

Typically, closed porosity (P_C) and total porosity (P_T) could be calculated based on the Eqs. (4) and (5).

$$P_C=1-D_a/\rho_{Theoretical} \quad (4)$$

$$P_T=P_O+P_C \quad (5)$$

Since the theoretical density ($\rho_{Theoretical}$) of sintered pellet is difficult to be determined accurately due to the unstable lithium stoichiometry and experiment error, it was replaced with specified value in this case to calculate the relative closed porosity (P_{RC}) and relative total porosity (P_{RT}).

2.3 Ionic conductivity measurement

Total ionic conductivity (σ) was measured by electrochemical impedance spectroscopy (EIS) with PARSTAT 4000A (U.S. AMETEK Princeton Applied Research) in a frequency range from 10 MHz to 1 Hz with an amplitude of 50 mV, and the data were fitted with ZView and calculated by

$$\sigma=L/(RS) \quad (6)$$

where L, S and R are thickness, surface area and fitted-resistance of the solid-state electrolyte ceramic pellet, respectively. Activation energy (E_a) was calculated in a temperature range of 283−333 K based on the Arrhenius Law as

$$\sigma=A\exp[-E_a/(RT)] \quad (7)$$

Before measuring conductivity, the pellets were polished and sputtered with Au as current collector with JFC−1600 (Japan JEOL).

3 Results and discussion

3.1 Crystal phase and porosity of inorganic solid-state electrolytes

Cubic phase garnet type solid-state electrolyte materials have been considered as the fast ion conductive composition. Figure 1 shows the XRD result of pellets prepared under different sintering conditions. All of the samples were identical and the main phase matched the typical cubic phase $Li_5La_3Nb_2O_{12}$ (PDF No. 80-0457). The primary concern about long-time sintering at high temperatures was that the lacking-lithium mixed phase, typically $La_2Zr_2O_7$ (PDF No. 71-2363), would be easily produced. However, no clear patterns of $La_2Zr_2O_7$ emerged in these samples, which indicated that the as- employed powder-covering method was feasible to prepare garnet type solid-state electrolytes.

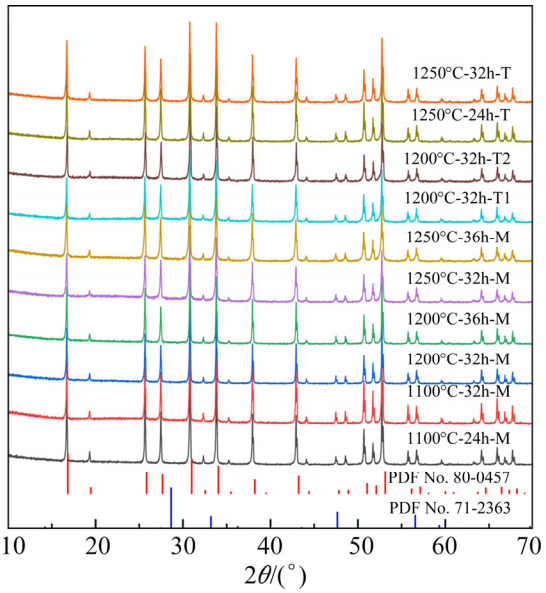

Fig. 1 XRD patterns of samples prepared under different sintering conditions

Figure 2 displays cross-section morphology and porosity of the sintered ceramic pellets. As observed, the pores generally decreased as sintering temperature was elevated and sintering duration was prolonged. However, this characterization was partial since the observed parts were only fragments of the pellets and it was difficult to quantify porosity. Thus, pycnometry was taken advantage to measure the open porosity, apparent density and bulk density directly and then calculate closed porosity and total porosity. To calculate closed porosity and total porosity, theoretical density has to be determined accurately. AGUESSE et al [20] utilized 5.15 g/cm^3 as the theoretical density for Ga-doped $Li_7La_3Zr_2O_{12}$. After referring to the crystal parameters from the work from WU et al [21] by means of neutron powder diffraction refinement, the theoretical density of $Li_{6.4}Ga_{0.2}La_3Zr_2O_{12}$ could be calculated to be 5.17 g/cm^3. However, the

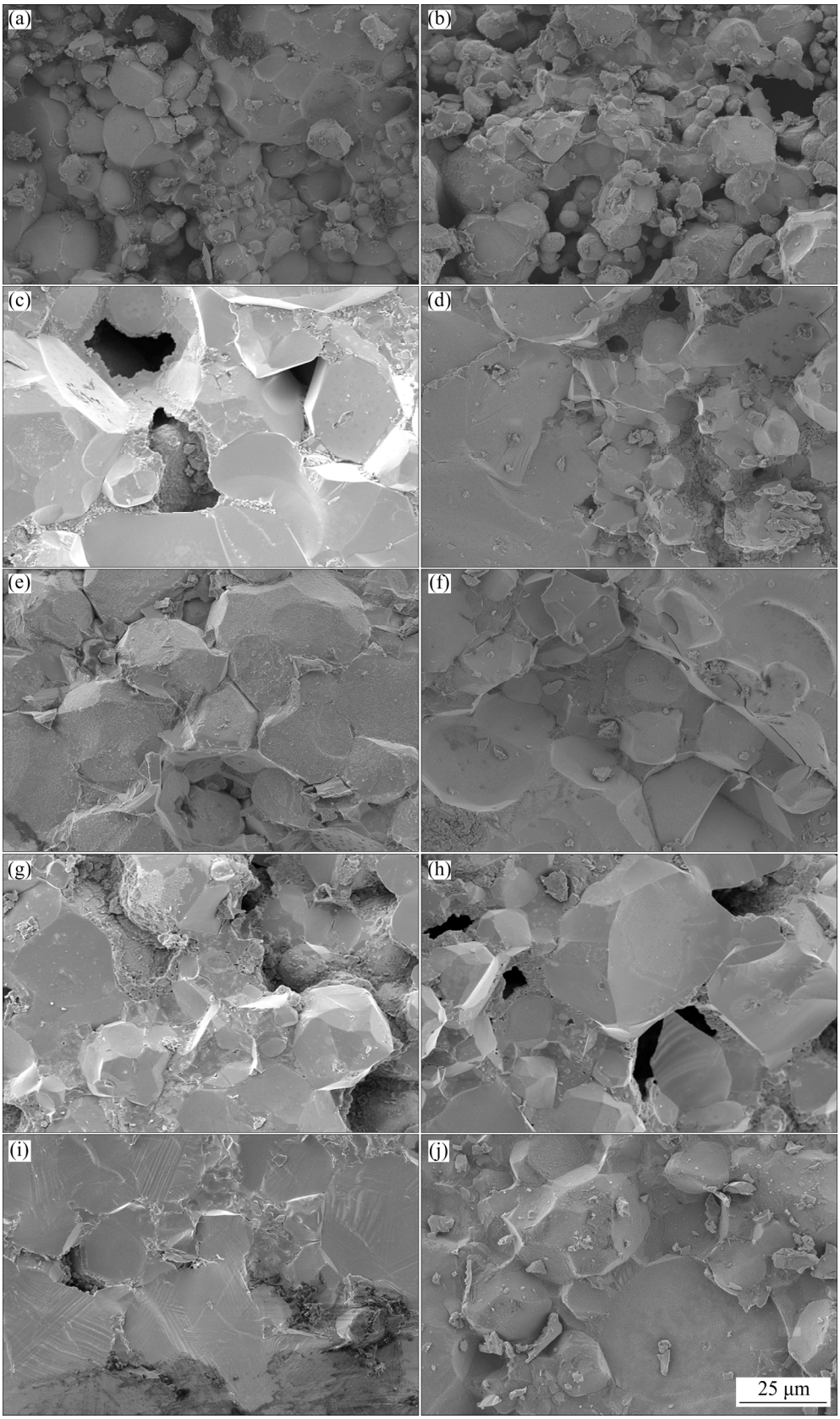

Fig. 2 Cross-section morphology of as-prepared pellets: (a) 1100°C-24h-M; (b) 1100°C-32h-M; (c) 1200°C-32h-M; (d) 1200°C-36h-M; (e) 1250°C-32h-M; (f) 1250°C-36h-M; (g) 1200°C-32h-T1; (h) 1200°C-32h-T2; (i) 1250°C-24h-T; (j) 1250°C-32h-T

Li:Ga:La:Zr molar ratio from ICP-OES result was 7.02:0.19:3:1.95, which showed a disagreement with the refinement result. In this case, 1250°C-32h-M sample was chosen to measure its molar ratio. The fact that the molar ratio of Li:Ga:La:Zr from the ICP-OES result in Table 1 was 6.66:0.20:3:1.95 demonstrated this inconsistency again. No matter whether the real composition of the sintered pellets was $Li_{6.4+2\delta}Ga_{0.2}La_3Zr_2O_{12+\delta}$ or $\delta Li_2O + Li_{6.4}Ga_{0.2}La_3Zr_2O_{12}$, it was not appropriate to view 5.17 g/cm^3 as theoretical density. Moreover, some of the apparent density values from this series of experiments exceeded 5.17 g/cm^3, which led to difficulty of calculating closed porosity and suggested the accidental and systematic experiment error when measuring the small solid-state electrolytes for solid-state lithium batteries. Given the small volume of these sintered pellets typically with a diameter of 13−15 mm and a thickness of 2−3 mm, the hindsight accidental experiment error estimation was made and the maximum error of apparent density and open porosity were 8% and 2%, respectively. The systematic experiment error mainly resulted from temperature variation during measuring. Therefore, relative closed porosity (P_{RC}) and relative total porosity (P_{RT}) were introduced to reduce the influence of experiment error and calculated based on Eqs. (4) and (5) with the theoretical density replaced by a specified value, i.e., the maximum experimental apparent density 5.55 g/cm^3 in this work. The calculated result is shown in Fig. 3.

Table 1 Designed and characterized Li:Ga:La:Zr molar ratio of nominal $Li_{6.4}Ga_{0.2}La_3Zr_2O_{12}$

Molar ratio		Source
Designed	Characterized	
6.4:0.2:3:2	6.66:0.20:3:1.95	This work
6.4:0.2:3:2	7.02:0.19:3:1.95	Ref. [21]

3.2 Ionic conductivity and activation energy of inorganic solid-state electrolytes

Results of EIS measured at 303 K of the as-prepared samples are exhibited in Figs. 4(a) and (b). In a complete EIS spectra, the intercept of high frequency on the real axis is considered as the resistance of bulk and the following semicircle is believed to be the resistance of grain boundary. The arc at lower frequency is related to the electrode process. Considering the impedance in high frequencies as the signal representing the ion conduction in solid-state electrolyte was demonstrated by previous reports [22−24]. Specifically, the distance from zero to the intercept of the tail with the real axis could be assigned to the total resistance of solid-state electrolyte after referring to the work by LI et al [25]. In this work, two types of equivalent circuits (R_{total})-(R_2CPE2)(R_3CPE3) and (R_b)(R_{gb}CPE1)(R_2CPE2)-(R_3CPE3) were utilized to fit the experimental data to obtain total ionic conductivity since some of the samples did not exhibit a complete semicircle in high frequency range. Figures 4(c, d) give the Arrhenius plot. It was obvious that all the samples obeyed the Arrhenius relationship well. The calculated E_a is listed in Table 2.

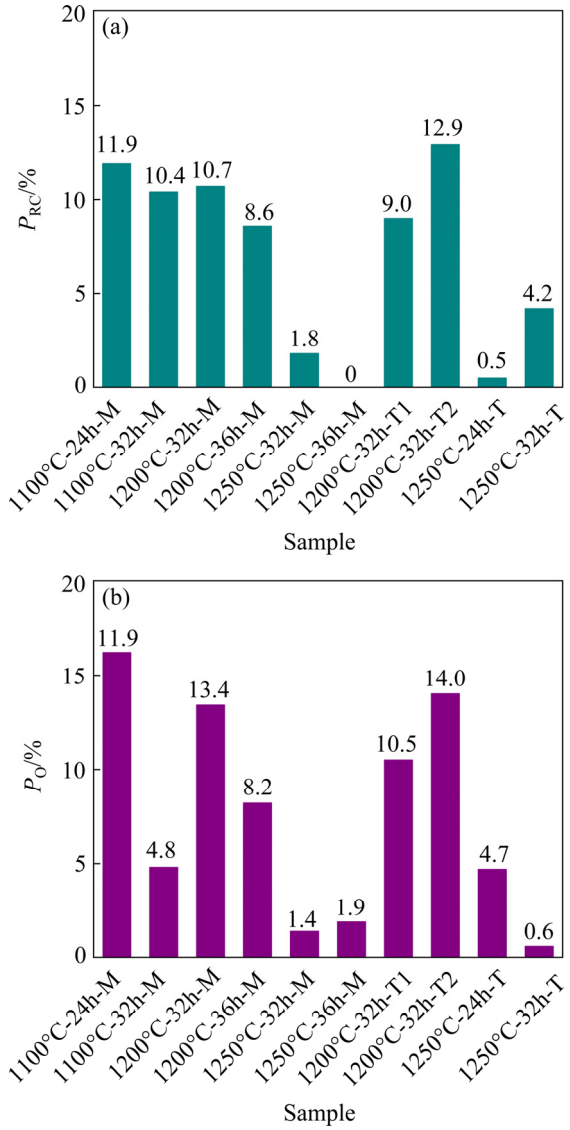

Fig. 3 Calculated relative closed porosity (P_{RC}) with 5.55 g/cm^3 as specified value (a), and open porosity (P_O) (b) of samples

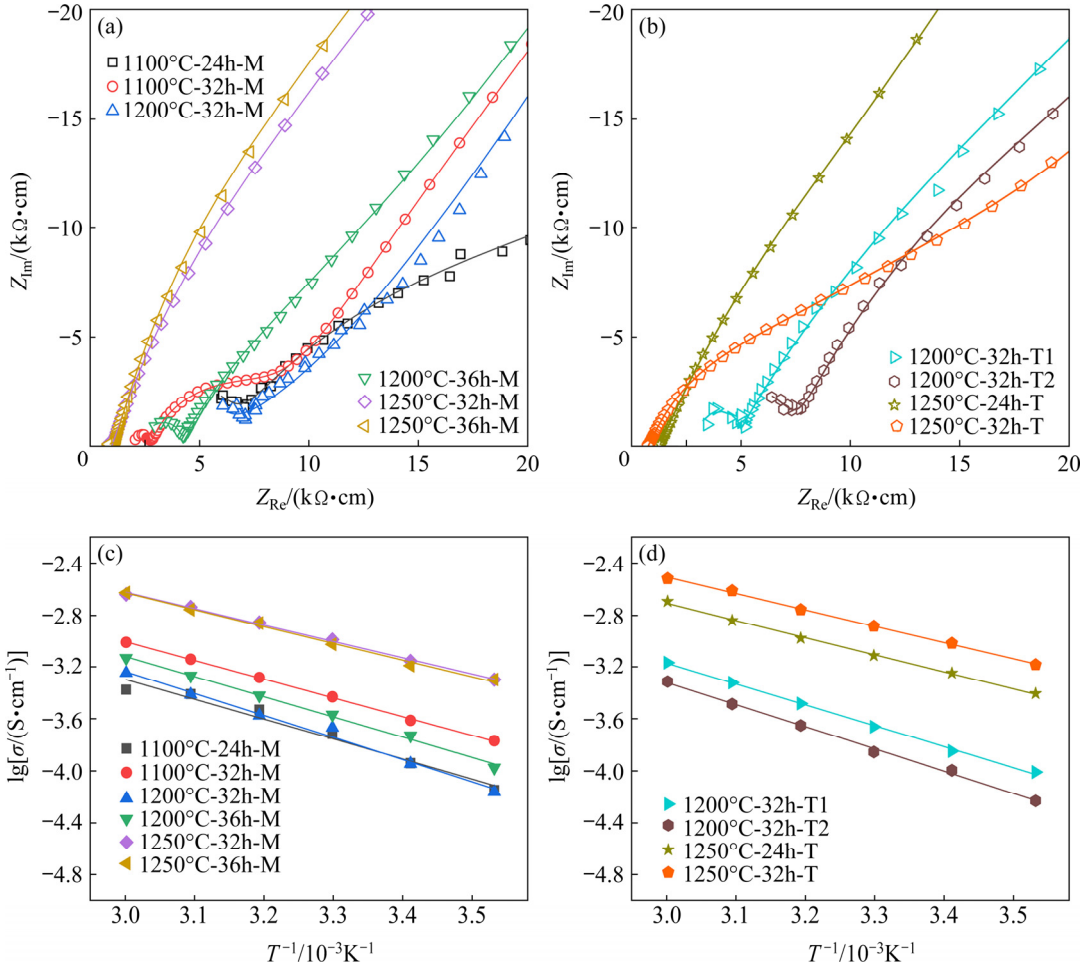

Fig. 4 EIS results of samples treated at 303 K for creating model (a) and verifying model (b), and Arrhenius plots of samples for creating model (c) and verifying model (d)

Table 2 Ionic conductivity at varied temperatures and activation energy of samples

Sample	Ionic conductivity/(mS·cm^{-1})						E_a/eV
	283 K	293 K	303 K	313 K	323 K	333 K	
1100°C-24h-M	0.07	0.11	0.19	0.30	0.39	0.42	0.31
1100°C-32h-M	0.17	0.24	0.37	0.52	0.73	0.98	0.29
1200°C-32h-M	0.07	0.11	0.22	0.27	0.39	0.57	0.34
1200°C-36h-M	0.11	0.19	0.27	0.38	0.54	0.74	0.31
1250°C-32h-M	0.51	0.70	1.03	1.40	1.83	2.29	0.25
1250°C-36h-M	0.51	0.65	0.95	1.39	1.75	2.36	0.26
1200°C-32h-T1	0.10	0.14	0.22	0.33	0.48	0.68	0.32
1200°C-32h-T2	0.06	0.10	0.14	0.22	0.33	0.49	0.34
1250°C-24h-T	0.39	0.57	0.78	1.06	1.45	2.02	0.26
1250°C-32h-T	0.66	0.97	1.31	1.75	2.44	3.02	0.25

3.3 Relationship between ionic conductivity and open porosity

With quantitative data, mathematical model can be exploited to analyze the relationship between porosity and ionic conductivity. Firstly, plots of ionic conductivity at 303 K versus relative closed porosity, relative total porosity and open porosity were separately plotted as shown in Fig. 5 and

Fig. 6(a). It was clear that ionic conductivity generally decreased when porosity increased. The easily recognizable decay pattern emerged separately between ionic conductivity versus relative total porosity and open porosity. But the most explicit decay relationship was the one between ionic conductivity and open porosity.

Since there are so many mathematical models that can explain this explicit relationship, "simple principle" is taken into account. For instance,

$$y=A_1\exp(-x/T_1)+A_2 \tag{8}$$

$$y=A_1\exp(-x/T_1)+A_2\exp(-x/T_2)+A_3 \tag{9}$$

where x and y are independent variable P_O and

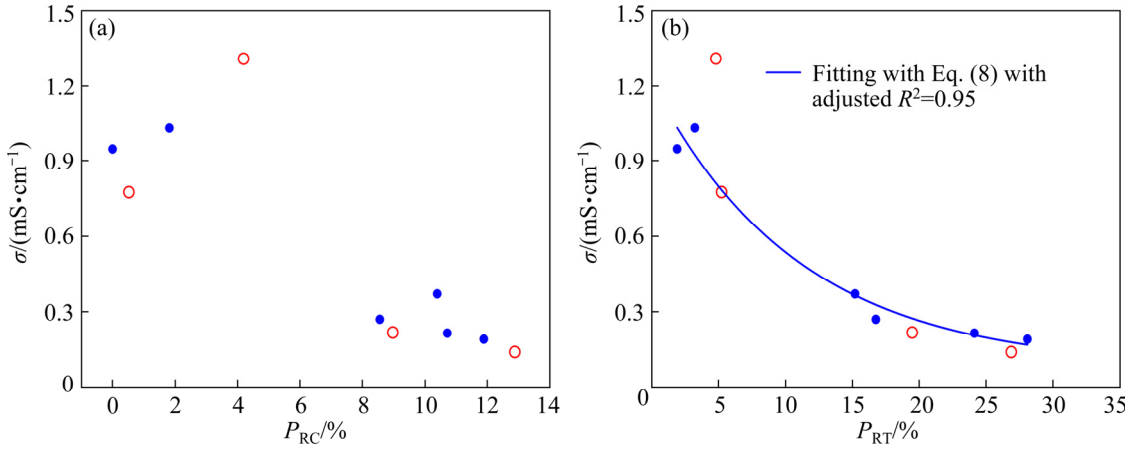

Fig. 5 Plots of ionic conductivity at 303 K versus relative closed porosity (a) and relative total porosity (b) (The blue solid circles are to create model and the red open circles are to verify it)

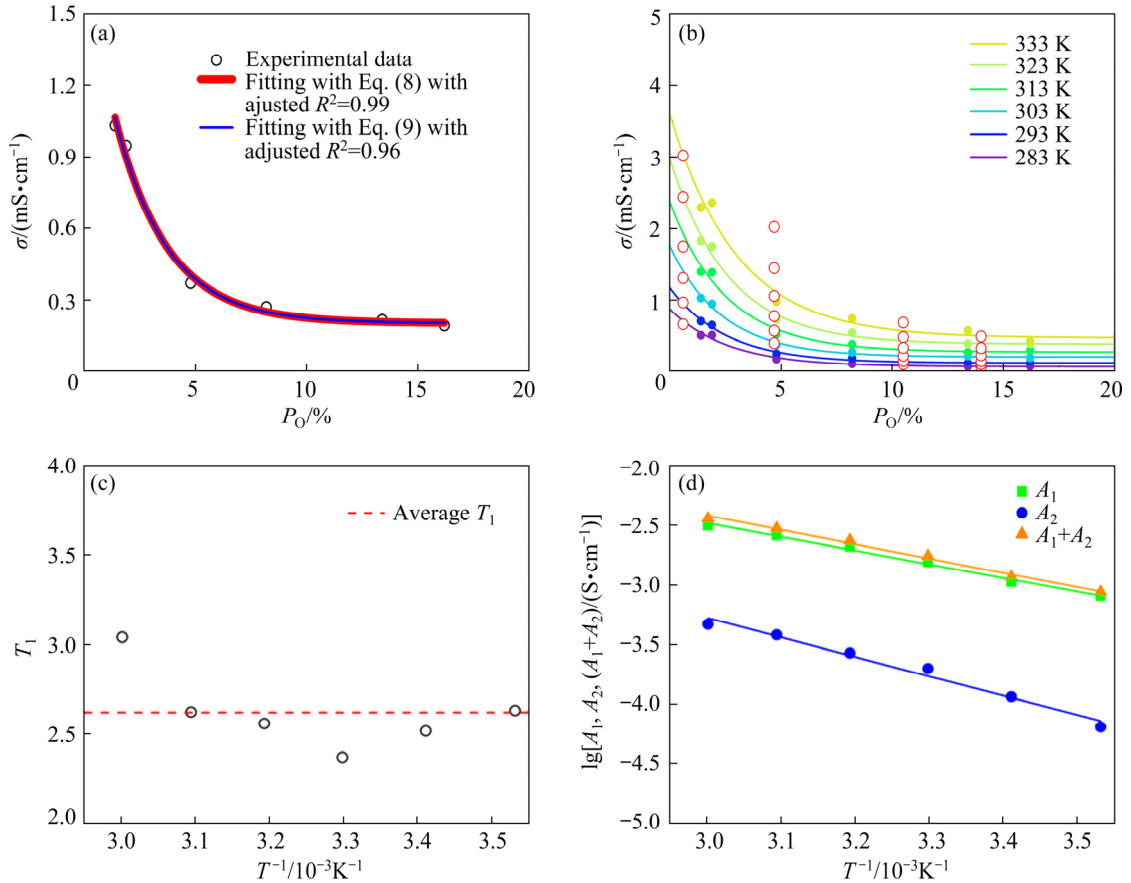

Fig. 6 Fitting results with exponential decay model and properties of parameters: (a) Comparison of fitting with Eqs. (8) and (9); (b) Testifying fitting result of Eq. (8) (The red open circles are to testify as-created model); (c) Relationship of T_1 versus temperature; (d) Relationship of A_1, A_2 and (A_1+A_2) versus temperature

dependent variable σ, and A_1, A_2, A_3, T_1 and T_2 are certain constants at given temperature. The two equations fitted so well with experiment data at the same time that indeed these two fitting curves totally coincided as shown in Fig. 6(a), the simpler Eq. (8) was chosen as the thoroughly studied one. Ionic conductivity and open porosity data at other temperatures were also fitted with Eq. (8), and the fitting results are shown in Fig. 6(b) and Table 3. All of the fitting curves showed over 0.95 of adjusted R^2 value. It manifested that a good fitting model was found. Furthermore, the other four samples were then brought in to testify Eq. (8) as shown in Fig. 6(b). Although the data of 1250°C-24h-T sample deviated from fitting curves, those of the remaining three samples almost accurately lied on the fitting curves. This suggests that the exponential decay relationship between ionic conductivity and open porosity is probably satisfied but needs correction later.

If Eq. (8) was applicable to this case, dimensional analysis method was then introduced, so that this mathematical model could be converted into a physicochemical model with the parameters embodying real meanings. Since x represents open porosity, T_1 must be a decay constant related to open porosity with the same unit. While y reflects ionic conductivity, A_1 and A_2 must be referred to two process of ion conduction with S/cm as unit. Moreover, if T_1 refers to a constant, it will not change so much against temperature. And if A_1 and A_2 refer to conductivity of ion conduction, then they must obey the Arrhenius law. Figures 6(c) and (d) are the relationships of T_1, A_1, A_2 and (A_1 + A_2) versus temperature. T_1 appeared to fluctuate around a constant that was averaged to be 2.62%. What was striking was that not only did A_1 and A_2 obey the Arrhenius law quite well but also (A_1+A_2) evidently obeyed it. Activation energy of assumed conductivity of A_1, A_2 and (A_1+A_2) was also calculated to be 0.23, 0.33 and 0.24 eV. Therefore, according to what is discussed, Eq. (8) can be rewritten as

$$\sigma=\sigma_1\exp(-P_O/P_{Cons})+\sigma_2 \quad (10)$$

where σ represents the total ionic conductivity of a given solid-state electrolyte material at a given temperature; P_{Cons} represents a constant of open porosity, which is possibly affected by the shape and distribution of the open pores; σ_1 and σ_2 represent ionic conductivity of two certain conduction process, which might be related to the chemical composition and grain arrangement.

3.4 Correction of relationship between ionic conductivity and porosity

Based on the understanding of ion conduction, both open pores and closed pores are detrimental to ionic conductivity. Revisiting Fig. 5(b), the exponential decay relationship between relative total porosity and ionic conductivity is also clear. This doubt leads to a hypothesis that open porosity is proportional to total porosity (P_T) as

$$P_T=kP_O \quad (11)$$

where k is the proportional coefficient. In this way, Eq. (10) can be revised as

$$\sigma=\sigma_1\exp[-P_T/(kP_{Cons})]+\sigma_2 \quad (12)$$

Since k is also a constant, it will not change the exponential decay pattern at all. In our case, the relationship of P_O and P_{RT} was explored as observed in Fig. 7(a). Considering experiment error and data fluctuation, confidence band was introduced to assist analyzing. With the increment of confidence level, more and more data points were comprised and 90% prediction band included

Table 3 Fitting results with Eq. (8)

T/K	A_1/(10^{-3} S·cm^{-1})		T_1		A_2/(10^{-4} S·cm^{-1})		Adjusted R^2
	Value	Standard error	Value	Standard error	Value	Standard error	
283	0.81	0.12	2.63	0.70	0.64	0.28	0.97
293	1.06	0.12	2.52	0.47	1.16	0.24	0.98
303	1.56	0.16	2.37	0.39	2.01	0.29	0.99
313	2.10	0.33	2.56	0.68	2.70	0.69	0.97
323	2.60	0.30	2.62	0.53	3.82	0.67	0.98
333	3.13	0.48	3.04	0.93	4.68	1.45	0.96

all of them. The intercept of the fitting line was 1.61 instead of 0 and the origin point nearly lied on the lower prediction limit line of 40% prediction band, which reveals that the relationship between relative total porosity and open porosity is more likely to be

$$P_{RT}=kP_O+b \quad (13)$$

where b is the intercept. Noticing that 1100°C-32h-M and 1250°C-24h-T samples were possible outliers, linear relationship of relative total porosity and open porosity was explored further after regrouping them in Fig. 7(b). The result implies that different sintering conditions will lead to different linear patterns. To verify Eq. (13) furthermore, another four large pellets aiming to reduce the relative error were prepared. Its relative total porosity was calculated twice with 5.55 g/cm^3 and 5.17 g/cm^3 as specified value. The relationship between relative total porosity and open porosity is also displayed in Fig. 7(b). The excellent linear relationship elucidates that the relationship of relative total porosity and open porosity is confirmed to be what Eq. (13) expresses. Additionally, the similar linear patterns of small pellets sintered at 1250 °C and large pellets sintered at 1250 °C demonstrate that different sintering conditions will lead to different linear patterns from another perspective. However, it was a pity that the crystal phase of larger pellets was difficult to be identically cubic with good crystallinity as shown in Fig. 8, and that their ionic conductivity could not be stably obtained to exemplify Eq. (10) furthermore.

If Eq. (13) is applicable to describe the relationship between relative total porosity and open porosity, the extrapolated value of relative total porosity will not be zero when open porosity reaches zero. When open porosity reaches zero, Eq. (10) could further be simplified as

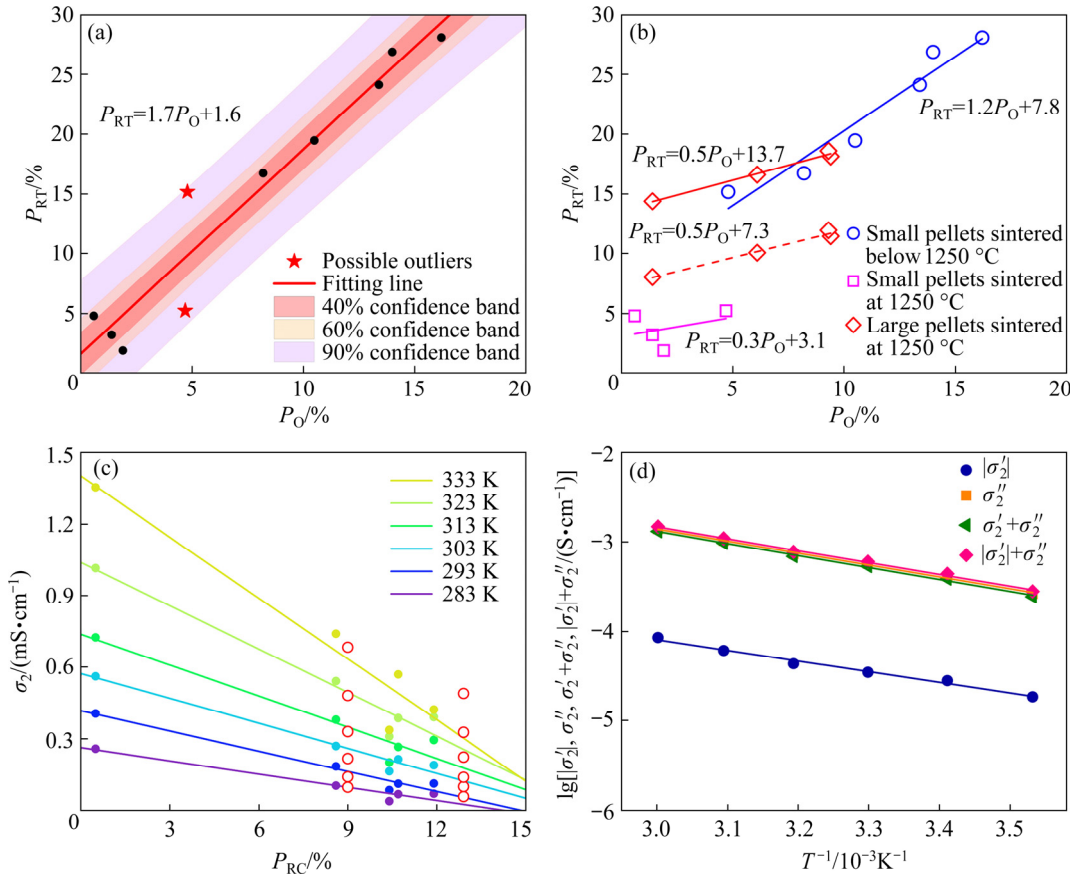

Fig. 7 (a) Linear relationship of open porosity and relative total porosity with confidence band; (b) Regrouped linear relationship of open porosity and relative total porosity (fitted dash line explains the data with 5.17 g/cm^3 as the specified density value of pellet to calculate relative total porosity, the other solid lines explain the data with 5.55 g/cm^3 as the specified density value of pellet to calculate relative total porosity); (c) Linear relationship of relative closed porosity and σ_2' (the red open circles are to testify it); (d) Arrhenius plots of $|\sigma_2'|$, σ_2'', $\sigma_2'+\sigma_2''$ and $|\sigma_2'|+\sigma_2''$ (σ_2' is the slope, and σ_2'' is the intercept. Since the numerical value of σ_2' is negative, the Arrhenius plot of σ_2' is calculated based on its absolute value)

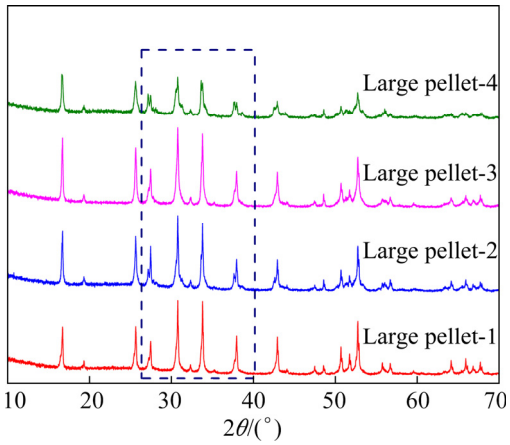

Fig. 8 XRD patterns of four large pellets sintered at 1250 °C for 32 h

$$\sigma=\sigma_1+\sigma_2 \tag{14}$$

suggesting that the two certain ion conduction processes will follow the same rule under such circumstances. This leads to another hypothesis that σ_2 is related to the effect of closed porosity on ionic conductivity, since P_O=0 can be viewed as P_C=0 in the open-pore region. Thus, why the ionic conductivity of 1100°C-32h-M sample with an open porosity of 4.8% and 1250°C-24h-T sample with an open porosity of 4.7% varied much could also be explained well with this hypothesis since their closed porosity was of great difference.

To find out the relationship between σ_2 and closed porosity, a series of electrolytes with the same open porosity but remarkably different closed porosity have to be prepared, which seems to be impossible to realize in reality. In our case, only 1100°C-32h-M and 1250°C-24h-T samples have very close open porosity and different relative closed porosities. Their σ_2 values could be stripped by subtracting $\sigma_1\exp(-P_O/P_{Cons})$ from σ with the help of the obtained fitting parameters. But data of only two samples are clearly not enough. For a typical exponential decay relationship,

$$y=A\exp(-x/T) \tag{15}$$

where A and T are constants.

When x is over $3T$, the decrement of y will be more than 95%. Therefore, σ_2 of the samples with large open porosity could be approximately equal to total ionic conductivity value. Several stripped and approximate σ_2 values are shown in Table 4. The relationship between σ_2 and relative closed porosity is displayed in Fig. 7(c). Even though the result was not ideal, the relationship between σ_2 and relative closed porosity was determined to be a linear one.

$$\sigma_2=\sigma'_2P_{RC}+\sigma''_2 \tag{16}$$

The fitting results are listed in Table 5. Again, dimensional analysis method was brought in and the Arrhenius plots of $|\sigma'_2|$, σ''_2, $\sigma'_2+\sigma''_2$ and $|\sigma'_2|+\sigma''_2$ were established well in Fig. 7(d). Activation energy of $|\sigma'_2|$ and σ''_2 was calculated to be 0.24 and 0.27 eV, respectively. Ultimately, the relationship between porosity and ionic conductivity was adjusted to be

$$\sigma=\sigma_1\exp(-P_O/P_{Cons})+\sigma'_2P_C+\sigma''_2 \tag{17}$$

This result suggests that open pores and closed pores have different effects on ion conduction, which would make sense since their boundary conditions are very distinctive. A study regarding the effect on the electrical resistivity of carbon materials illustrated that an increase of the open porosity by 40% leads to a resistivity increase by 250% while the same increase in closed porosity gives rise to a resistivity of only 25%, calculated based on ideal fluid mechanics model and verified with experiment data [26]. This reflects that different types of pores in conductors need to be treated differently. Moreover, it is important to

Table 4 σ_2 values at different temperatures with different methods (10^{-4} S·cm^{-1})

Sample	283 K	293 K	303 K	313 K	323 K	333 K	Method
1100°C-32h-M	0.40	0.86	1.65	2.02	3.10	3.37	Strip
1250°C-24h-T	2.59	4.05	5.61	7.25	10.18	13.53	Strip
1100°C-24h-M	0.71	1.14	1.91	2.95	3.90	4.21	Approximate
1200°C-32h-M	0.69	1.13	2.15	2.66	3.86	5.69	Approximate
1200°C-36h-M	1.05	1.86	2.70	3.79	5.41	7.41	Approximate
1200°C-32h-T1	0.98	1.42	2.18	3.30	4.80	6.84	Approximate
1200°C-32h-T2	0.59	1.01	1.40	2.24	3.27	4.89	Approximate

The first five samples are used to create linear relationship, and 1200°C-32h-T1 and 1200°C-32h-T1 samples are used to testify it

Table 5 Fitting results with Eq. (16)

T/K	σ'_2/(10^{-5} S·cm^{-1})		σ''_2/(10^{-4} S·cm^{-1})		Adjusted R^2
	Value	Standard error	Value	Standard error	
283	−1.84	0.17	2.64	0.25	0.92
293	−2.80	0.32	4.16	0.30	0.95
303	−3.47	0.37	5.73	0.34	0.96
313	−4.34	0.72	7.39	0.67	0.90
323	−6.09	0.79	10.40	0.74	0.94
333	−8.52	1.33	14.00	1.25	0.91

density solid-state electrolytes for higher ionic conductivity. Special sintering approaches, such as hot-pressing sintering and spark plasma sintering, are advantageous methods. To further understand the effect of porosity better and deeper on ionic conductivity in this case, theoretical model must be established in future to unravel the detailed meanings of P_{Cons}, σ_1, σ'_2 and σ''_2. Fluid dynamics mechanics might be a solution, which is the research topic in the forthcoming work.

4 Conclusions

(1) Open porosity causes ionic conductivity to decrease exponentially. The pre-exponential factor obeys the Arrhenius Law quite well with the activation energy of 0.23 eV, and the decay constant is averaged to be 2.62%.

(2) Closed porosity causes ionic conductivity to decrease linearly. The slope and intercept of this linear pattern also obey the Arrhenius Law, whose activation energies are 0.24 and 0.27 eV, respectively.

(3) Total porosity is linearly dependent on the open porosity. Different sintering conditions will lead to different linear patterns with different slopes and intercepts.

Acknowledgments

This work was supported by the Innovation and Entrepreneurship Project of Hunan Province, China (No. 2019GK5053), Program of Huxiang Young Talents, China (No. 2019RS2002), the Natural Science Foundation for Distinguished Young Scholars of Hunan Province, China (No. 2020JJ2047), and the Fundamental Research Funds for the Central Universities of Central South University, China.

References

[1] DONG Ming-xia, LI Xiang-qun, WANG Zhi-xing, LI Xin-hai, GUO Hua-jun, HUANG Zhen-jun. Enhanced cycling stability of La modified $LiNi_{0.8-x}Co_{0.1}Mn_{0.1}La_xO_2$ for Li-ion battery [J]. Transactions of Nonferrous Metals Society of China, 2017, 27: 1134−1142.

[2] GUO Hua-jun, LI Xiang-qun, HE Fang-yong, LI Xin-hai, WANG Zhi-xing, PENG Wen-jie. Effects of sodium substitution on properties of $LiMn_2O_4$ cathode for lithium ion batteries [J]. Transactions of Nonferrous Metals Society of China, 2010, 20: 1043−1048.

[3] DUNN B, KAMATH H, TARASCON J M. Electrical energy storage for the grid: A battery of choices [J]. Science, 2011, 334: 928−935.

[4] CASTELVECCHI D, STOYE E. Chemistry Nobel honours world-changing batteries [J]. Nature, 2019, 574: 308.

[5] MANTHIRAM A. A reflection on lithium-ion battery cathode chemistry [J]. Nature Communications, 2020, 11: 1550.

[6] LARCHER D, TARASCON J M. Towards greener and more sustainable batteries for electrical energy storage [J]. Nature Chemistry, 2015, 7: 19−29.

[7] JANEK J, ZEIER W G. A solid future for battery development [J]. Nature Energy, 2016, 1: 16141.

[8] XU Lin, TANG Sun, CHENG Yu, WANG Kang-yan, LIANG Ji-yuan, LIU Cui, CAO Yuan-cheng, WEI Feng, MAI Li-qiang. Interfaces in solid-state lithium batteries [J]. Joule, 2018, 2: 1991−2015.

[9] ZHANG Jun, ZHENG Chao, LI Lu-jie, XIA Yang, HUANG Hui, GAN Yong-ping, LIANG Chu, HE Xin-ping, TAO Xin-yong, ZHANG Wen-kui. Unraveling the intra and intercycle interfacial evolution of Li_6PS_5Cl-based all-solid-state lithium batteries [J]. Advanced Energy Materials, 2020, 10: 1903311.

[10] LOU Jia-tao, WANG Guo-guang, XIA Yang, LIANG Chu, HUANG Hui, GAN Yong-ping, TAO Xin-yong, ZHANG Jun, ZHANG Wen-kui. Achieving efficient and stable interface between metallic lithium and garnet-type solid electrolyte through a thin indium tin oxide interlayer [J]. Journal of Power Sources, 2020, 448: 227440.

[11] MANTHIRAM A, YU Xing-wen, WANG Shao-fei. Lithium battery chemistries enabled by solid-state electrolytes [J]. Nature Reviews Materials, 2017, 2: 16103.

[12] CHEN Ru-song, LI Qing-hao, YU Xi-qian, CHEN Li-quan, LI Hong. Approaching practically accessible solid-state batteries: Stability issues related to solid electrolytes and interfaces [J]. Chemical Reviews, 2020, 120: 6820−6877.

[13] ZHENG Feng, KOTOBUKI M, SONG Shu-feng, LAI M O, LU Li. Review on solid electrolytes for all-solid-state lithium-ion batteries [J]. Journal of Power Sources, 2018, 389: 198−213.

[14] KRAFT M A, OHNO S, ZINKEVICH T, KOERVER R, CULVER S P, FUCHS T, SENYSHYN A, INDRIS S, MORGAN B J, ZEIER W G. Inducing high ionic conductivity in the lithium superionic argyrodites $Li_{6+x}P_{1-x}Ge_xS_5I$ for all-solid-state batteries [J]. Journal of the

American Chemical Society, 2018, 140: 16330−16339.
[15] KATO Y, HORI S, SAITO T, SUZUKI K, HIRAYAMA M, MITSUI A, YONEMURA M, IBA H, KANNO R. High-power all-solid-state batteries using sulfide superionic conductors[J]. Nature Energy, 2016, 1: 16030.
[16] AONO H, SUGIMOTO E, SADAOKA Y, IMANAKA N, ADACHI G Y. Ionic conductivity of solid electrolytes based on lithium titanium phosphate [J]. Journal of the Electrochemical Society, 1990, 137: 1023−1027.
[17] ZHANG Xing-xing, OH T S, FERGUS J W. Densification of Ta-doped garnet type $Li_{6.75}La_3Zr_{1.75}Ta_{0.25}O_{12}$ solid electrolyte materials by sintering in a lithium-rich air atmosphere [J]. Journal of the Electrochemical Society, 2019, 166: A3753−A3759.
[18] GAO Yuan, SUN Shu-yang, ZHANG Xin, LIU Yong-feng, HU Jian-jiang, HUANG Zhen-guo, GAO Ming-xia, PAN Hong-ge. Amorphous dual-layer coating: Enabling high Li-ion conductivity of non-sintered garnet type solid electrolyte [J]. Advanced Functional Materials, 2021, 31: 2009692.
[19] MURUGAN R, THANGADURAI V, WEPPNER W. Fast lithium ion conduction in garnet−type $Li_7La_3Zr_2O_{12}$ [J]. Angewandte Chemie International Edition, 2007, 46: 7778−7781.
[20] AGUESSE F, MANALASTAS W, BUANNIC L, LOPEZ DEL AMO J M, SINGH G, LLORDÉS A, KILNER J A. Investigating the dendritic growth during full cell cycling of garnet electrolyte in direct contact with Li metal [J]. ACS Applied Materials & Interfaces, 2017, 9: 3808−3816.
[21] WU Jian-fang, CHEN En-yi, YU Yao, LIU Lin, WU Yue, PANG Wei-kong, PETERSON V K, GUO Xin. Gallium-doped $Li_7La_3Zr_2O_{12}$ garnet-type electrolytes with high lithium-ion conductivity [J]. ACS Applied Materials & Interfaces, 2017, 9: 1542−1552.
[22] BUSCHMANN H, DÖLLE J, BERENDTS S, KUHN A, BOTTKE P, WILKENING M, HEITJANS P, SENYSHYN A, EHRENBERG H, LOTNYK A, DUPPEL V, KIENLE L, JANEK J. Structure and dynamics of the fast lithium ion conductor "$Li_7La_3Zr_2O_{12}$" [J]. Physical Chemistry Chemical Physics, 2011, 13: 19378−19392.
[23] KUMAZAKI S, IRIYAMA Y, KIM K H, MURUGAN R, TANABE K, YAMAMOTO K, HIRAYAMA T, OGUMI Z. High lithium ion conductive $Li_7La_3Zr_2O_{12}$ by inclusion of both Al and Si [J]. Electrochemistry Communications, 2011, 13: 509−512.
[24] BERNUY L C, MANALASTAS W, LOPEZ D A J M, AGUADERO A, AGUESSE F, KILNER J A. Atmosphere controlled processing of Ga-substituted garnets for high Li-ion conductivity ceramics [J]. Chemistry of Materials, 2014, 26: 3610−3617.
[25] LI Yu-tao, HAN Jian-tao, WANG Chang-an, XIE Hui, GOODENOUGH J B. Optimizing Li^+ conductivity in a garnet framework [J]. Journal of Materials Chemistry, 2012, 22: 15357−15361.
[26] SUN Tian-ming, DONG Li-min., WANG Chen, GUO Wen-li, WANG Li, LIANG Tong-xiang. Effect of porosity on the electrical resistivity of carbon materials [J]. New Carbon Materials, 2013, 28: 349−354.

石榴石型无机固态电解质中离子电导率与气孔率之间的经验衰减关系

郭志豪[1,2,3]，李新海[1,2,3]，王志兴[1,2,3]，郭华军[1,2,3]，彭文杰[1,2,3]，胡启阳[1,2,3]，颜果春[1,2,3]，王接喜[1,2,3]

1. 中南大学 冶金与环境学院，长沙 410083；
2. 中南大学 先进电池材料教育部工程研究中心，长沙 410083；
3. 中南大学 有色金属增值冶金湖南省重点实验室，长沙 410083

摘 要：离子电导率是无机固态电解质的一个非常重要的性能指标。为了探究气孔率与离子电导率之间的关系，通过固相法制备一系列不同气孔率的 $Li_{6.4}Ga_{0.2}La_3Zr_2O_{12}$ 石榴石型无机固态电解质。基于量化的数据并借助数学模型和量纲分析方法，提出气孔率与离子电导率之间的经验衰减关系并对其进行讨论。结果表明，开气孔率以指数效力方式造成离子电导率衰减，其指前因子遵循阿伦尼乌斯定律且激活能为 0.23 eV，平均衰减常数为 2.62%。闭气孔率以线性效力方式造成离子电导率衰减，斜率和截距也遵循 Arrhenius 定律，其激活能分别为 0.24 eV 和 0.27 eV。另外，总气孔率与开气孔率之间存在线性依赖关系，且不同的烧结制度导致不同截距和斜率的线性特征。

关键词：石榴石型无机固态电解质；离子电导率；气孔率；经验衰减关系

(Edited by Xiang-qun LI)